Synthesis and physical properties of (Zr1−x,Tix)3AlC2MAX phases

Zapata-Solvas, E, Hadi, M, Horlait, D, Parfitt, D, Thibaud, A, Chroneos, A & Lee, W

DOI 10.1111/jace.14870
ISSN 0002-7820
ESSN 1551-2916
Publisher: Wiley

Received: 5 January 2017 | Accepted: 1 March 2017

DOI: 10.1111/jace.14870

ORIGINAL ARTICLE

Journal of the American Ceramic Society

Synthesis and physical properties of $(Zr_{1-x},Ti_x)_3AlC_2$ MAX phases

Eugenio Zapata-Solvas[1] | Mohammad A. Hadi[2] | Denis Horlait[1,3] | David C. Parfitt[4] | Axel Thibaud[1] | Alexander Chroneos[1,4] | William E. Lee[1]

[1]Centre for Nuclear Engineering (CNE) & Department of Materials, Imperial College London, London, UK

[2]Department of Physics, University of Rajshahi, Rajshahi, Bangladesh

[3]CNRS/IN2P3 and University of Bordeaux, Centre d'Etudes Nucléaires de Bordeaux-Gradignan, UMR 5797, Gradignan, France

[4]Faculty of Engineering, Environment and Computing, Coventry University, Coventry, UK

Correspondence
Eugenio Zapata-Solvas, Centre for Nuclear Engineering (CNE) & Department of Materials, Imperial College London, London, UK.
Email: Eugenio.zapata-solvas@imperial.ac.uk
Alexander Chroneos, Faculty of Engineering, Environment and Computing, Coventry University, Coventry, UK.
Email: Alexander.chroneos@imperial.ac.uk

Abstract

MAX phase solid solutions physical and mechanical properties may be tuned via changes in composition, giving them a range of possible technical applications. In the present study, we extend the MAX phase family by synthesizing $(Zr_{1-x}Ti_x)_3AlC_2$ quaternary MAX phases and investigating their mechanical properties using density functional theory (DFT). The experimentally determined lattice parameters are in good agreement with the lattice parameters derived by DFT and deviate <0.5% from Vegard's law. Ti_3AlC_2 has a higher Vickers hardness as compared to Zr_3AlC_2, in agreement with the available experimental data.

KEYWORDS

DFT, MAX phases, Synthesis

1 | INTRODUCTION

$M_{n+1}AX_n$ phases (n=integer, M=early transition metal; A=group 13-16 element and X=C or N) were initially investigated in the 1960s,[1] however, the interest of the community was captured by a study on the remarkable properties of Ti_3SiC_2 nearly two decades ago.[2,3] $M_{n+1}AX_n$ phases exhibit the $P6_3/mmc$ (no. 194) space group.[1,2] The first (n=1) and second (n=2) members of the family are known as the 211 and 312 MAX phases respectively. A feature of them is the highly symmetric unit cell with atomic layers stacked along the *c*-direction. Numerous MAX phases were synthesized that shared these metallic and ceramic properties (good machinability, high melting temperature, high thermal shock resistance, high elastic stiffness, high thermal, and electrical conductivity), effectively motivating their technological application.[2-5] The key for the metallic and ceramic properties is the structure that consists of the stacking of $M_{n+1}X_n$ "ceramic" layer(s) interleaved by an A "metallic" layer.[2-5]

Ti-based MAX phases such as Ti_3AlC_2 are of significant technical interest as they have excellent properties combined with a strong oxidation resistance in air due to formation of a passivating Al_2O_3 outer layer.[6] Related MAX phases have been investigated as candidate materials for passive safety protection of nuclear fuel cladding (i.e.

in accident scenarios as occurred at Fukushima, Japan).[7-12] For example, in the Accident-Tolerant Fuel (ATF) concept there is a requirement to protect the nuclear fuel cladding material (a Zr-based alloy) against oxidation for tens of hours at temperatures exceeding 1200°C.[10] Ti_3AlC_2 is considered as it has good oxidation resistance but also low neutron absorption cross section.[13] For the same application $Zr_{n+1}AlC_n$ MAX phases are attractive because Zr-containing phases will likely adapt better onto current Zr-based alloys in nuclear fuel cladding in addition to having comparatively lower neutron absorption cross section. All in all, the whole $(Zr_{1-x},Ti_x)_3AlC_2$ quaternary system is worthy of study as a promising system to design properties depending on industry demands.

Indeed quaternary MAX phases have attracted research interest as there is potential to fine tune the properties of a given MAX phase.[14-20] For example, the right amount of Ge added to Cr_2AlC allowed the resulting MAX phase solid solution to display an isotropic thermal expansion.[21] Examination of the compositional flexibility of 312 MAX phases in addition to characterization of their structure and understanding of their physical properties is needed. However, the difficulty of getting single-phase MAX phases (or even with a yield higher than 90 wt%) is a current challenge, which needs to be addressed since, for example, the maximum yield reported for Zr_3AlC_2 is only 59 wt%.[12] In addition, it is still unclear whether Zr_3AlC_2 could be formed as a pure ternary or if it needs addition of impurities such as Si to assist the nucleation process and/or to stabilize Zr_3AlC_2.[22]

The aim of the present study is to investigate the synthesis and mechanical properties of the $(Zr_{1-x}Ti_x)_3AlC_2$ quaternary MAX phases. Lattice parameters calculated by density functional theory (DFT) are compared with those determined by X-ray diffraction (XRD) of fabricated ceramics.

2 | METHODOLOGY

2.1 | Experimental method

Commercial reactants used were ZrH_2 grade S (APS 2-4 μm, >99.7%, Rockwood Lithium, Frankfurt, Germany), Al (−325 mesh, >99.9%, Alfa Aesar, Heysham, UK), TiH_2 grade T (APS ~3.5 μm, >99.9%, Rockwood Lithium, Frankfurt, Germany), and C (>99.9%, Sigma Aldrich, Dorset, UK). Elemental mixtures for Zr_3AlC_2 were prepared with stoichiometries for the 312 phase adjusted to 3/1.1/1.9 for Zr/Al/C to compensate for partial Al sublimation and C uptake from the graphite die during sintering,[8] as is usually done for MAX phase syntheses.

Powder mixtures were prepared in a glove box under a controlled atmosphere of Ar. Then, the powder mixtures were dry-milled to break up agglomerates and produce homogeneous mixing in a planetary ball mill PM-100 (Retzch, Han, Germany) in a polyvinyl jar sealed inside the glove box for 30 minutes at 150 rpm, which is a speed high enough to produce an homogeneous mixing and break agglomerates but low enough to avoid contamination from the media. Milling was performed in a dry environment with 10 mm diameter ZrO_2 balls (Grade TZ-3Y, Tosoh, Japan) as milling media. Finally, the powders were precompacted at 20 MPa in a 30 mm diameter graphite die, which was placed in a hot-press HP W/25/1 (FCT Systeme, Frankenblick, Germany) and heated to 1450°C for 60 minutes under an applied pressure of 30 MPa to produce the MAX phase in the $(Zr_{1-x},Ti_x)_3AlC_2$ quaternary system. A dwell time of 60 minutes was found to be optimum as shorter or longer dwells reduce the yield of the MAX phases formed. Sintering was performed at an intermediate temperature of 1450°C to form solid solutions in the $(Zr_{1-x},Ti_x)_3AlC_2$ quaternary system, considering that the temperature to produce Zr_3AlC_2 is 1500°C[12] and Ti_3AlC_2 is 1400°C.[23]

A PANalytical instrument was used for X-Ray diffraction (XRD) studies, using a 0.02° 2Θ step and an angular range from 5 to 100°. Crystalline phase determination was carried out using International Center for Diffraction Data database (ICDD)[24] and the Xpert High Score plus software (PANalytical, Almelo, the Netherlands) for phase matching.[25] Determination of lattice parameters was carried out using a full-pattern matching method (Le Bail function) with the help of the Fullprof suite program.[25] Finally, phase ratios were determined by Rietveld refinement using Xpert High Score software. Sample observations on polished cross sections with 1 μm surface finish, were carried out in a scanning electron microscope (SEM) Auriga (Zeiss, Oberkochen, Germany), under back-scattering electron (BSE) and secondary electron (SE) imaging modes, equipped with an energy-dispersive spectroscopy (EDS) detector with ultra-thin polymer window (Oxford Instruments, Oxford, UK).

2.2 | Theoretical method

The plane wave DFT code CASTEP,[26] was used with exchange and correlation interactions being formulated by employing the corrected density functional of Perdew, Burke and Ernzerhof (PBE)[27] in the generalized gradient approximation (GGA) and in conjunction with ultrasoft pseudopotentials.[28] The virtual crystal approximation (VCA) was used initially to model disorder in these cells; this is an effective medium method that can be used to model disordered alloys.[29] In VCA disorder is introduced by assigning partial occupancies to each atomic site of the disordered sublattice. A disadvantage of the technique is the assumption of a homogeneous distribution of atoms on

the disordered sublattice and this does not consider the possibility of clustering. For all the VCA calculations, the unit cell was relaxed to a stress of less than 50 MPa using the algorithm of Pfrommer et al.,[30] with a plane wave basis set cutoff of 450 eV and a 4×4×1 Monkhorst-Pack (MP)[31] k-point grid which was sufficient to give a converged accuracy of 0.1 eV per formula unit. Traditional point defect calculations were performed to check the VCA values and examine the antisite defects Ti_{Zr} and Zr_{Ti} (i.e. replacement of host metal atoms by the opposite) in 1×1×1 (12 atoms), 2×2×1 (48 atoms) and 3×3×1 (108 atoms) cells using a similar or smaller k-point spacing and the same energy cut-off. The minimum defect-defect separation in these cells is 1*a*, 2*a,* and 3*a* (*a*~3 Å) and so they are representative of single compositions within the phase diagram rather than an infinitely dilute limit. Increasing the cut-off energy to 650 eV and decreasing the k-point spacing to 0.025 $Å^{-1}$ resulted in a change in the final cell volume of a 3×3×1 supercell defect calculation of 0.013 $Å^3$ per formula unit which we consider to be inconsequential to the quality of comparison with diffraction data.

3 | RESULTS AND DISCUSSION

3.1 | Structural properties

The phase compositions of the obtained samples were determined using XRD (Figure 1), by performing XRD refinements (Table 1) and with the help of SEM and EDS measurements (Figure 2). Crystalline phase determination by XRD (Figure 1) first revealed the formation of $(Zr_{1-x},Ti_x)_3AlC_2$ MAX phases as well as ZrC or TiC over the whole range studied. In addition, XRD peaks corresponding to 211 MAX phases were detected in the targeted compositions $Zr_{2.5}Ti_{0.5}AlC_2$, Zr_2TiAlC_2, $Zr_{1.5}Ti_{1.5}AlC_2$, and $ZrTi_2AlC_2$, which suggests the possibility of obtaining solid solutions in the 211 system and this will be the subject of a further study. Figure 2 shows SEM microstructures of compositions Zr_2TiAlC_2, $Zr_{1.5}Ti_{1.5}AlC_2$ and $ZrTi_2AlC_2$ and the different EDS spectra used to quantify the real stoichiometry of $(Zr_{1-x},Ti_x)_3AlC_2$ MAX phases. One or two phases with lamellar structure are seen in each sample, visually confirming the formation of MAX phases. EDS was used to determine the obtained *x* values in the 312 MAX phases. For the $ZrTi_2AlC_2$ sample, the accumulation of EDS point measurements revealed the presence of two different *x*=Ti/(Zr+Ti) ratios, the major one being *x*=0.80, the other *x*=0.45. To differentiate the 211 and the 312 MAX phases, the lattice parameters of the 312 and 211 quaternary phases were compared to those of ternary end-members (Table 1). It was then evident, as confirmed by Figure 3, that the 312 MAX phase was the Ti-rich one (*x*=0.8), while the 211 was Zr-rich (*x*=0.45). Table 1 reports the compositions of the 312 quaternary MAX phase synthesized. It was found that samples $Zr_{2.5}Ti_{0.5}AlC_2$, Zr_2TiAlC_2 and $Zr_{0.5}Ti_{2.5}AlC_2$ led to actual compositions fairly close to those targeted. However, for $Zr_{1.5}Ti_{1.5}AlC_2$ and $ZrTi_2AlC_2$ the deviations were greater: $Zr_{1.5}Ti_{1.5}AlC_2$ was low in Ti as the composition $(Zr_{0.56}Ti_{0.44})_3AlC_2$ was determined by EDS and conversely $ZrTi_2AlC_2$ was found with an excess of Ti ($(Zr_{0.20}Ti_{0.80})_3AlC_2$ measured). These observations may be due to the existence of a miscibility gap in the $(Zr_{1-x},Ti_x)_3AlC_2$ system for x values in the $0.45<x<0.80$ range. This would also explain the formation of ZrC and a Zr-rich 211 MAX phase in the $ZrTi_2AlC_2$ sample to accommodate Zr (and Al and C) excess(es). By extension, the present results suggest also that contrary to the analogous $(Cr_{1-x}Ti_x)_3AlC_2$[9,32] and $(Mo_{1-x}Ti_x)_3AlC_2$[33] systems, there is no formation of a $(Zr_{2/3}Ti_{1/3})_3AlC_2$ compound stabilized by ordering of the Zr and Ti cations on the respective 4*f* and 2*a* Wyckoff sites. Table 1 also reports the lattice parameters determined for $(Zr_{1-x},Ti_x)_3AlC_2$, $(Zr_{1-x},Ti_x)_2AlC$, ZrC, and TiC phases. The lattice parameters for ZrC are similar to the lowest reported for ZrC,[34] which suggests that highly substoichiometric ZrC_{1-x} is formed (with $x\approx0.4$),[34] and/or that some substitution of Zr by Ti occurs. Conversely, TiC only found in the $Zr_{0.5}Ti_{2.5}AlC_2$ sample, has a rather high unit cell parameter (4.362 Å) compared to its usual value (4.328 Å) and should therefore contain some Zr. More importantly, it could be seen in Table 1 that there is a gradual decrease in the lattice parameters of the 312 MAX phases from Zr_3AlC_2 to Ti_3AlC_2, in agreement with the formation of $(Zr_{1-x},Ti_x)_3AlC_2$ solid solutions.

In Table 1, we also report the synthesis yields. The MAX phase $(Zr_{0.15}Ti_{0.85})_3AlC_2$ was produced with a 94 wt % yield with only TiC as a secondary phase. The other

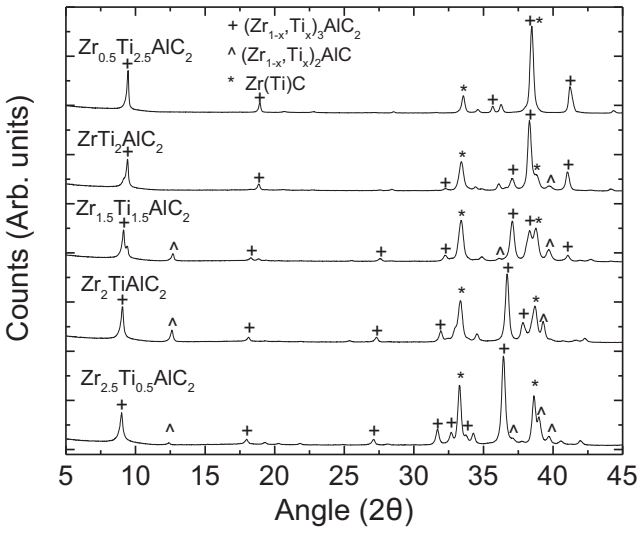

FIGURE 1 X-ray diffractograms of $(Zr_{1-x}Ti_x)_3AlC_2$ quaternary MAX phases

TABLE 1 Lattice parameters of $(Zr_{1-x},Ti_x)_3AlC_2$ MAX phases and of secondary phases $(Zr_{1-x},Ti_x)_2AlC$ and (Zr,Ti)C

Sample (Targeted compound)	Phases (composition from EDS)	Space groups	Unit cell parameters				Phase ratio[a] (wt%)
			a (Å)	b (Å)	c (Å)	V (Å^3)	
Zr_3AlC_2[22]	Zr_3AlC_2	$P6_3/mmc$	3.3287 (4)	3.3287 (4)	20.011 (1)	192.01 (6)	7 (1)
$Zr_{2.5}Ti_{0.5}AlC_2$	$(Zr_{0.815}Ti_{0.185})_3AlC_2$	$P6_3/mmc$	3.2900 (4)	3.2900 (4)	19.696 (4)	184.63 (8)	61 (2)
	Zr(Ti)C	$Fm\bar{3}m$	4.6597 (6)	4.6597 (6)	4.6597 (6)	4.6597 (6)	39 (2)
Zr_2TiAlC_2	$(Zr_{0.69}Ti_{0.31})_3AlC_2$	$P6_3/mmc$	3.2674 (5)	3.2674(5)	19.572(4)	180.96(6)	41(2)
	$(Zr,Ti)_2AlC$	$P6_3/mmc$	3.184 (1)	3.184(1)	14.046(4)	123.3(4)	30(2)
	Zr(Ti)C	$Fm\bar{3}m$	4.6523 (9)	4.6523(9)	4.6523(9)	100.70(3)	29(2)
$Zr_{1.5}Ti_{1.5}AlC_2$	$(Zr_{0.56}Ti_{0.44})_3AlC_2$	$P6_3/mmc$	3.2317 (9)	3.2317(9)	19.397(5)	175.44(9)	51(2)
	$(Zr,Ti)_2AlC$	$P6_3/mmc$	3.148 (1)	3.148(1)	13.93(6)	119.6(5)	26(2)
	Zr(Ti)C	$Fm\bar{3}m$	4.646 (1)	4.646(1)	4.646(1)	100.28(4)	23(2)
$ZrTi_2AlC_2$	$(Zr_{0.20}Ti_{0.80})_3AlC_2$	$P6_3/mmc$	3.1276 (8)	3.1276(8)	18.816(4)	159.40(7)	69(2)
	Zr(Ti)C	$Fm\bar{3}m$	4.642 (1)	4.642(1)	4.642(1)	100.05(6)	31(2)
$Zr_{0.5}Ti_{2.5}AlC_2$	$(Zr_{0.15}Ti_{0.85})_3AlC_2$	$P6_3/mmc$	3.1156 (5)	3.1156 (5)	18.750 (4)	157.62 (5)	94 (1)
	Ti(Zr)C	$Fm\bar{3}m$	4.3623 (1)	4.3623 (1)	4.3623 (1)	83.013 (5)	6 (1)
Ti_3AlC_2[38]	Ti_3AlC_2	$P6_3/mmc$	3.0786 ()	3.0786 ()	18.73 ()	153.736 ()	

[a]For phase ratio determination, very minor phases (eg. 211 MAX phase in $Zr_{2.5}Ti_{0.5}AlC_2$) had to be excluded. This is expected to have a very limited effect on the calculated values.

samples led to MAX phase yields (312 and 211 combined) of 61 to 77 wt% and the minimum yield for a 312 MAX phase was obtained for $(Zr_{0.69}Ti_{0.31})_3AlC_2$ (41 wt%). The recent discovery of Zr_3AlC_2 and Zr_2AlC_2 by Lapauw et al.[12,35] has raised some questions about the mechanism of their synthesis, as others investigators were unable to synthesize them.[8] Lapauw et al.[12,35] suggested that the choice of ZrH_2 powders as a reactant in their work could have led to the formation of Zr_3AlC_2 and Zr_2AlC_2 and highlighted the need for further study.[35] It is well-known that impurities play a key role in the nucleation of MAX phases, for example the deliberate addition of a small amount of Si (~1 to 4 at.%) in the reaction powder mix of Ti_3AlC_2 leads to significant yield, purity, and grain size improvements.[36-39] Furthermore, it has been demonstrated recently that addition of 1.6 at.% of Si leads to an increased MAX phase yield from 7 wt% to 59 wt% in Zr_3AlC_2,[22] which is exactly the same yield reported by Lapauw et al.[12] using an impurity-rich (including Si) ZrH_2 powder reactant. The nucleation was presumably assisted by the presence of Zr_5Si_3 particles in an analogous manner to how Ti_5Si_3 has been found to enhance the nucleation of Ti_3AlC_2.[36] In the present study it is significant that a composition such as $Zr_{2.5}Ti_{0.5}AlC_2$ can be produced with a 61 wt% yield while, using similar experimental conditions with the same reactants, Zr_3AlC_2 barely forms (7 wt%).[22] It may thus be inferred that the presence of Ti assists nucleation and/or growth of $(Zr_{1-x},Ti_x)_3AlC_2$ and/or that Ti integration in Zr_3AlC_2 somehow favors the MAX phase formation rather than of competing phases.

Figure 3 combines the above-discussed results by plotting for the considered $(Zr_{1-x}Ti_x)_3AlC_2$ quaternary MAX phases the experimental and VCA-calculated lattice parameters as a function of the EDS-determined x values, revealing good agreement between the experimental and VCA values. We also considered point defect calculations of Ti_{Zr} and Zr_{Ti} defects in $1\times1\times1$, $2\times2\times1$ and $3\times3\times1$ cells and the calculated lattice parameter range is very close to the experimental lattice parameters. A way to assess this is by Vegard's law which is an empirical rule stating that a property of an alloy (here we consider lattice parameters) can be calculated from a linear interpolation of the property values of its constituent elements (or for higher order alloys, constituent compounds).[40,41] In essence the lattice parameters are in good agreement with Vegard's Law as their fractional deviation from the line drawn between the end-members' values is only up to 0.5% (refer to Figure 4) except for the c lattice parameter of $(Zr_{0.20}Ti_{0.80})_3AlC_2$ which has a deviation of 1%. These deviations from Vegard's law may suggest some tendency for Zr-Ti ordering and this should be addressed using extensive supercells. Lapauw et al.[42] determined the formation of solid solutions in the $(Nb_{1-x},Zr_x)_4AlC_3$ quaternary system with $x\leq0.5$ and observed a deviation from Vegard's law above x=0.185, which is similar with the present study as $x\geq0.2$ here deviates from Vegard's Law (up to 1%). However, it was concluded that there was a solid solubility limit for Zr additions x>0.185 as the fraction of (Nb,Zr)C increased. In addition, lattice parameters a and c experimentally observed for x>0.185 followed a nonlinear-opposite bowing

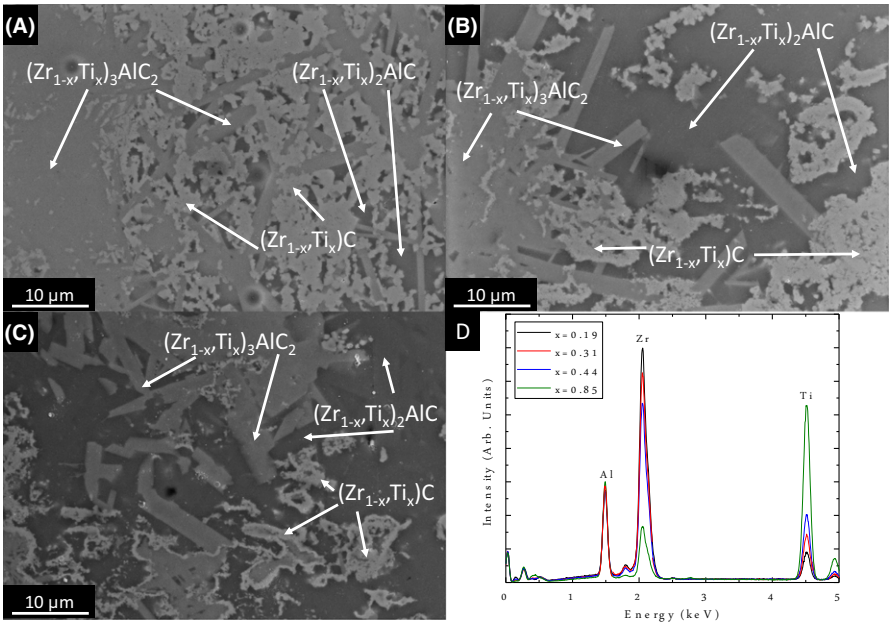

FIGURE 2 SEM micrographs of different $(Zr_{1-x}Ti_x)_3AlC_2$ quaternary MAX phases (A-C) and EDS spectra for different x stoichiometries; (A) Zr_2TiAlC_2, (B) $Zr_{1.5}Ti_{1.5}AlC_2$, (C) $ZrTi_2AlC_2$, (D) EDS spectra. $(Zr_{1-x},Ti_x)_3AlC_2$, $(Zr_{1-x},Ti_x)_2AlC$ and $(Zr_{1-x},Ti_x)C$ label the different phases detected in each composition. Figure 2C illustrates the presence of $(Zr_{1-x},Ti_x)_2AlC$ in $ZrTi_2AlC_2$ but note that it was distributed unevenly in the microstructure [Color figure can be viewed at wileyonlinelibrary.com]

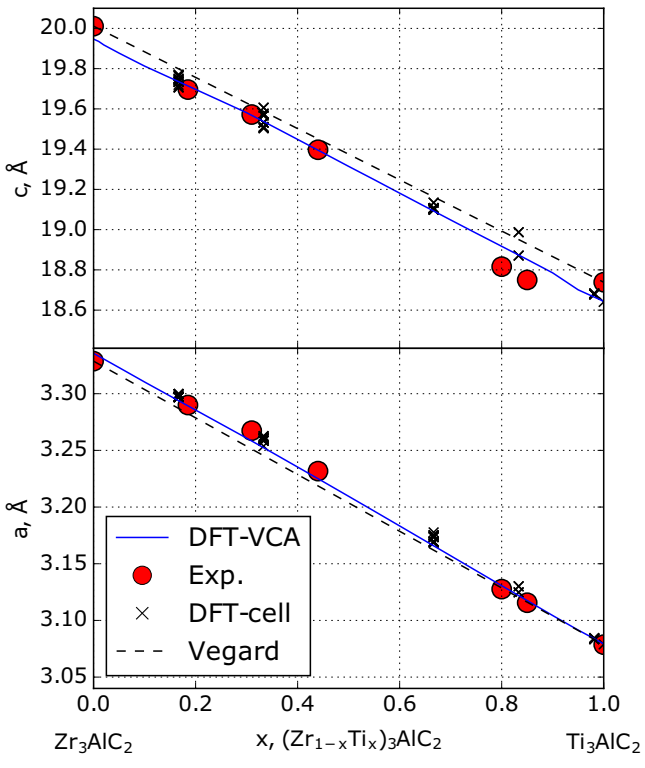

FIGURE 3 Determined and calculated lattice parameters of $(Zr_{1-x}Ti_x)_3AlC_2$ quaternary MAX phases. The DFT-cell data refers to point defect calculations of Ti_{Zr} and Zr_{Ti} defects [Color figure can be viewed at wileyonlinelibrary.com]

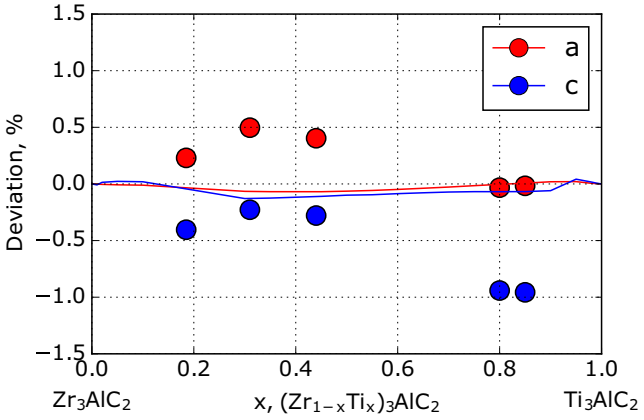

FIGURE 4 Fractional deviation from Vegard's law for the $(Zr_{1-x}Ti_x)_3AlC_2$ [Color figure can be viewed at wileyonlinelibrary.com]

trend above x>0.185 with a deviation of ~3%.[42] Figure 3 also graphically support the probable existence of a miscibility gap as we were not able to get a $(Zr_{1-x},Ti_x)_3AlC_2$ composition with 0.45<x<0.80, checked by EDS, despite targeting x values of x=0.5 and x=2/3.

3.2 | Population analysis and theoretical hardness

The population analysis in density functional theory using the CASTEP module is performed with a projection of the plane wave states onto a localized basis by means of a method

developed by Sanchez-Portal et al.[43] Population analysis of the resulting projected states is executed via the Mulliken formalism.[44] This method is extensively used in the analysis of electronic structure computations with the Linear Combination of Atomic Orbitals (LCAO) basis sets. In addition to providing a relevant condition in favor of bonding between atoms, the overlap population can be used to judge the covalent or ionic character of a bond. The bond population with a high value is a sign of a covalent bond, while a low value signifies an ionic interaction. The bonding and antibonding states are due to positive and negative bond overlap populations respectively. An additional gauge of ionic nature can be achieved from the effective ionic valence, which is computed as the difference between the formal ionic charge and the Mulliken charge on the anion species. If the value of effective valence is zero a perfectly ionic bond exists, while with values above zero the levels of covalency increase. The calculated Mulliken atomic populations and effective valence for nearest neighbors are presented in Table 2. Table 3 also lists the Mulliken bond number, bond length and bond overlap population of $(Zr_{1-x}Ti_x)_3AlC_2$ for x=0 and 1.

The effective valence indicates that the covalency in chemical bonding by the two end-members of MAX phase solid solutions $(Zr_{1-x}Ti_x)_3AlC_2$ is prominent with the level of covalency for these two compositions being similar. From the calculated bond population, it is seen that the Zr–C and Zr–Al bonds are slightly more covalent in Zr_3AlC_2 than the corresponding Ti–C and Ti–Al bonds in Ti_3AlC_2. Moreover, a bond between two Zr atoms in Zr_3AlC_2 arises with small negative populations but the similar Ti–Ti bond in Ti_3AlC_2 appears with large negative populations. The metallic population to bond population ratio $f_m=P^{\mu'}/P^{\mu}$ is used as a measure of metallicity of the chemical bond.[45,46] The calculated values of metallicity for the Ti1–C, Ti2–C and Ti–Al bonds in Ti_3AlC_2 are found to be 0.062, 0.082 and 0.150, whereas Zr1–C, Zr2–C, and Zr–Al bonds in Zr_3AlC_2 have respective values of 0.045, 0.062, and 0.079. It is evident that the bonds between transition metals and aluminum show a high degree of metallicity in both the end-members in comparison to the other bonds. In fact, the nature of bonding in the two end-members of $(Zr_{1-x}Ti_x)_3AlC_2$ MAX phases may be described as a combination of covalent and metallic.

TABLE 3 Calculated Mulliken bond number n^{μ}, bond length d^{μ}, and bond overlap population P^{μ} of μ-type bond of $(Zr_{1-x}Ti_x)_3AlC_2$ for x=0 and 1 (with their metallic populations in parenthesis)

Ti_3AlC_2 ($P^{\mu'}$=0.07208)				Zr_3AlC_2 ($P^{\mu'}$=0.05474)			
Bond	n^{μ}	d^{μ} (Å)	P^{μ}	**Bond**	n^{μ}	d^{μ} (Å)	P^{μ}
Ti1–C	4	2.07550	1.16	Zr1–C	4	2.25771	1.22
Ti2–C	4	2.19815	0.88	Zr2–C	4	2.38753	0.89
Ti–Al	4	2.90778	0.48	Zr–Al	4	3.07672	0.69
Ti–Ti	4	2.95899	−0.54	Zr–Zr	4	3.22779	−0.34
C–C	2	3.13896	−0.09	C–C	2	3.41744	−0.07

Gao[47] formulated equations to calculate the theoretical Vickers's hardness for nonmetallic compounds using Mulliken bond population within DFT. Although this method successfully predicts the hardness of a range of nonmetallic materials, it fails to evaluate the hardness of compounds having partial metallic bonding like MAX phases because of the delocalization of metallic bonding.[48] Gou et al.[45] introduced an additional term called metallic population to compensate the effect of delocalization of metallic bonding and reformulated Gao's equation as:

$$H_{\nu}^{\mu} = 740(P^{\mu} - P^{\mu'})(\nu_b^{\mu})^{-5/3}$$

where P^{μ} refers to the Mulliken overlap population of the μ-type bond, $P^{\mu'}$ is introduced for the metallic population and is evaluated from the unit cell volume V and the number of free electrons in a cell $n_{free} = \int_{E_P}^{E_F} N(E)dE$ as $P^{\mu'} = n_{free}/V$ and $\nu_b^{\mu}$is the volume of a bond of μ-type, which is calculated using the bond length d^{μ} of type μ and the number of bonds N_b^{ν} of type ν per unit volume with $\nu_b^{\mu} = (d^{\mu})^3 / \sum_{\nu}[(d^{\mu})^3 N_b^{\nu}]$. For complex multiband crystals, the hardness can be calculated as a geometric average of all bond harnesses using:[49,50]

TABLE 2 Population analysis of $(Zr_{1-x}Ti_x)_3AlC_2$ for x=0 and 1

		Mulliken atomic populations					
Compounds	**Species**	**s**	**p**	**d**	**Total**	**Charge (e)**	**Effective valence charge (e)**
Zr_3AlC_2	C	1.50	3.30	0.00	4.79	−0.79	–
	Al	1.15	1.93	0.00	3.08	−0.08	3.08
	Zr(1)	2.18	6.48	2.60	11.25	0.75	3.25
	Zr(2)	2.25	6.63	2.67	11.54	0.46	3.54
Ti_3AlC_2	C	1.48	3.25	0.00	4.73	−0.73	–
	Al	1.08	1.96	0.00	3.04	−0.04	3.04
	Ti(1)	2.13	6.62	2.61	11.35	0.65	3.35
	Ti(2)	2.17	6.75	2.65	11.58	0.42	3.58

TABLE 4 Calculated Vickers hardness H_v of $(Zr_{1-x}Ti_x)_3AlC_2$ for x=0 and 1 with the relevant quantities such as bond volume v_b^μ and bond hardnessH_v^μ

Compounds	Bond	n^μ	d^μ (Å)	P^μ	$P^{\mu'}$	v_b^μ (Å^3)	H_v^μ (GPa)	H_v (GPa)
Ti_3AlC_2	Ti–C	4	2.07550	1.16	0.07208	7.75556	26.49355	8.96
	Ti–C	4	2.19815	0.88	0.07208	9.21334	14.76516	
	Zr–Al	4	2.90778	0.48	0.07208	21.32699	1.84045	
Zr_3AlC_2	Zr–C	4	2.25771	1.22	0.05474	10.19784	17.98074	7.15
	Zr–C	4	2.38753	0.89	0.05474	12.06009	9.74546	
	Zr–Al	4	3.07672	0.69	0.05474	25.80880	2.08563	

$$H_V = \left[\prod^{\mu} (H_v^\mu)^{n^\mu}\right]^{\frac{1}{\sum n^\mu}}$$

where n^μ is the number of bond of type μ comprising the actual multiband crystal. The calculated values of the Vickers hardness for the two end compounds are listed in Table 4. The computed Vickers hardness values for Ti_3AlC_2 and Zr_3AlC_2 are 8.96 and 7.15 GPa respectively. For comparison, the experimental values are 11.4 and 4.4±0.4 GPa for Ti_3AlC_2 and Zr_3AlC_2 respectively.[12,51] Hardness values obtained from nanoindentation experiments carried out as a function of load (11.4 GPa for Ti_3AlC_2)[51] are larger than the early determined microhardness (in the range of 3-7 GPa for Ti_3AlC_2) values.[52-54] The present value is in good agreement with the previous theoretical values on Ti_3AlC_2.[55] Bei et al.[39] remarked that several grains are involved in the deformation process when indentation tests (micro- or nano-indentation) are performed with a large load. Consequently, the measured hardness values are likely affected by grain boundaries and impurities and this may explain the differences between the experimental and theoretical values.

4 | CONCLUSIONS

In the present study, we extend the MAX phase family by the synthesis of $(Zr_{1-x}Ti_x)_3AlC_2$ quaternary MAX phases. The derived and experimental lattice parameters are in agreement and both *a* and *c* lattice parameters were found to follow Vegard's law. It was, however, noted that no compositions were able to be experimentally obtained inside the $0.45<x<0.80$ range, suggesting the existence of a miscibility gap for this range. Ti_3AlC_2 is calculated to have a higher Vickers hardness as compared to Zr_3AlC_2, in agreement with the available experimental data.

FILES REPOSITORY

XRD raw data supporting this study can be found in Zenodo at https://doi.org/10.5281/zenodo.438016 and is openly available under a CC-BY license.

ACKNOWLEDGMENTS

E.Z.S, A.T., and W.E.L. work was funded as part of the EPSRC Carbides for Future Fission Environments (CAFFE) consortium (EP/M018563/1; EP/M018768/1). A.C. and D.C.P. are grateful for funding from the Lloyd's Register Foundation, a charitable foundation helping to protect life and property by supporting engineering-related education, public engagement, and the application of research.

REFERENCES

1. Nowotny H. Strukturchemie einiger verbindungen der ubergangsmetalle mit den elementen C, Si, Ge, S. *Prog Solid State Chem*. 1970;2:27-70.
2. Barsoum MW, Radovic M. Elastic and mechanical properties of the MAX Phases. *Annu Rev Mater Res*. 2011;41:195-227.
3. Barsoum MW, El-Raghy T. Synthesis and characterization of a remarkable ceramic: Ti_3SiC_2. *J Am Ceram Soc*. 1996;79:1953.
4. Barsoum MW, Brodkin D, El-Raghy T. Layered machinable ceramics for high temperature applications. *Scr Mater*. 1997;36:535.
5. Barsoum MW, Yaroschuck BG, Tyagi S. Fabrication and characterization of M_2SnC (M = Ti, Zr, Hf and Nb). *Scr Mater*. 1997;37:1583.
6. Tallman DJ, Anasori B, Barsoum MW. A critical review of the oxidation of Ti_2AlC, Ti_3AlC_2 and Cr_2AlC in Air. *Mater Res Lett*. 2013;1:115.
7. Middleburgh SC, Lumpkin GR, Riley D. Accommodation, accumulation, and migration of defects in Ti_3SiC_2 and Ti_3AlC_2 MAX phases. *J Am Ceram Soc*. 2013;96:3196.
8. Horlait D, Grasso S, Chroneos A, et al. Attempts to synthesise quaternary MAX phases (Zr, M)$_2$AlC and Zr$_2$(Al, A)C as a way to approach Zr_2AlC. *Mater Res Lett*. 2016;4:137.
9. Horlait D, Grasso S, Al Nasiri N, et al. Synthesis and high-temperature oxidation of MAX phases in the Cr-Ti-Al-C quaternary system, *J Am Ceram Soc*. 2016;99:682.
10. Bragg-Sitton S. Development of advanced accident tolerant fuels for commercial LWRs. *Nucl News*. 2014;83.
11. Horlait D, Middleburgh SC, Chroneos A, et al. Synthesis and DFT investigation of new bismuth-containing MAX phases. *Sci Rep*. 2016;6:18829.
12. Lapauw T, Halim J, Lu L, et al. Synthesis of the novel Zr_3AlC_2 MAX phase. *J Eur Ceram Soc*. 2016;36:943.

13. Hoffman EN, Vinson DW, Sindelar RL, et al. MAX phase carbides and nitrides: properties for future nuclear power plant in-core applications and neutron transmutation analysis. *Nucl Eng Des*. 2012;244:17.
14. Wang J, Zhou Y. Ab initio elastic stiffness of nano-laminate $(M_xM'_{2-x})AlC$ (M and M' = Ti, V and Cr) solid solution. *J Phys: Condens Matter*. 2004;16:2819.
15. Meng F, Zhou Y, Wang J. Strengthening of Ti_2AlC by substitution of Ti with V. *Scripta Mater*. 2005;53:1369.
16. Yeh CL, Chen JH. Combustion synthesis of $(Ti_{1-x}Nb_x)_2AlC$ solid solutions from elemental and Nb_2O_5/Al_4C_3-containing powder compacts. *Ceram Int*. 2011;37:3089.
17. Yeh CL, Yang WJ. Formation of MAX solid solutions (Ti, V)$_2$AlC and (Cr, V)$_2$AlC with Al_2O_3 addition by SHS involving aluminothermic reduction. *Ceram Int*. 2013;39:5737.
18. Jiao ZY, Wang TX, Ma SH. Phase stability, mechanical properties and lattice thermal conductivity of ceramic material $(Nb_{1-x}Ti_x)(4)AlC_3$ solid solutions. *J Alloys Compd*. 2016;687:47.
19. Gua J, Pan L, Yang J, et al. Mechanical properties and oxidation behavior of Ti-doped Nb_4AlC_3. *J Eur Ceram Soc*. 2016;36:1001.
20. Lin S, Huan Y, Zu L, et al. Alloying effects on structural, magnetic, and electrical/thermal transport properties in MAX-phase $Cr_{2-x}M_xGeC$ (M = Ti, V, Mn, Fe, and Mo). *J Alloys Compd*. 2016;680:452.
21. Cabioc'h T, Eklund P, Mauchamp V, et al. Tailoring of the thermal expansions of the MAX phases in the $Cr_2(Al_{1-x},Ge_x)C_2$ system. *J Eur Ceram Soc*. 2013;33:897.
22. Zapata-Solvas E, Christopoulos SRG, Ni N, et al. Experimental synthesis and DFT investigation of radiation tolerance of $Zr_3(Al_{1-x}Si_x)C_2$ MAX phases. *J Am Ceram Soc* Article accepted 15 Dec 2016. DOI: 10.1111/jace.14742
23. Zhou A, Wang CA, Huang Y. A possible mechanism on synthesis of Ti_3AlC_2. *Mater Sci Eng, A*. 2003;352:333.
24. Kabekkodu S. PDF-4. PA:ICDD: Newton Square; 2010.
25. Roisnel T, Rodriguez-Carvajal J. WinPLOTR: a windows tool for powder diffraction pattern analysis. *Mater Sci Forum*. 2011;378:118.
26. Segall MD, Lindan PJD, Probert MJ, et al. First-principles simulation: ideas, illustrations and the CASTEP code. *J Phys: Condens Matter*. 2002;14:2717.
27. Perdew J, Burke K, Ernzerhof M. Generalized gradient approximation made simple. *Phys Rev Lett*. 1996;77:3865.
28. Vanderbilt D. Soft self-consistent pseudopotentials in a generalized eigenvalue formalism. *Phys Rev B*. 1990;41:7892.
29. Yu CJ, Emmerich H. An efficient virtual crystal approximation that can be used to treat heterovalent atoms, applied to $(1-x)BiScO_3 - xPbTiO_3$. *J Phys: Condens Matter*. 2007;19:306203.
30. Pfrommer BG, Cote M, Louie SG, et al. Relaxation of crystals with the quasi-Newton method. *J Comput Phys*. 1997;131:233.
31. Monkhorst HJ, Pack JD. Special points for Brillouin-zone integrations. *Phys Rev B*. 1976;13:5188.
32. Liu Z, Wu E, Wang J, et al. Crystal structure and formation mechanism of $(Cr_{2/3}Ti_{1/3})_3AlC_2$ MAX phase. *Acta Mater*. 2014;73:186.
33. Anasori B, Halim J, Lu J, et al. Mo_2TiAlC_2: a new ordered layered ternary carbide. *Scripta Mater*. 2015;101:5.
34. Jackson H, Lee WE. Properties and characteristics of ZrC. *Compr Nucl Mater*. 2012;2:339-372.
35. Lapauw T, Lambrinou K, Cabioc'h T, et al. Synthesis of the new MAX phase Zr_2AlC. *J Eur Ceram Soc*. 2016;36:1847.
36. Xu X, Ngai TG, Li Y. Synthesis and characterization of quarternary $Ti_3Si_{(1-x)}Al_xC_2$ MAX phase materials. *Ceram Int*. 2015;41:7626.
37. Zhu J, Mei B, Xu X, et al. Synthesis of single-phase polycrystalline Ti_3SiC_2 and Ti_3AlC_2 by hot pressing with the assistance of metallic Al or Si.*Mater Lett*. 2004:58;588.
38. Zhou W, Mei B, Zhou J. Fabrication of high-purity ternary carbide Ti_3AlC_2 by spark plasma sintering (SPS) technique. *Ceram Int*. 2007;33:1399.
39. Bei GP, Gauthier-Brunet V, Tromas C, et al. Synthesis, characterization, and intrinsic hardness of layered nanolaminate Ti_3AlC_2 and $Ti_3Al_{0.8}Sn_{0.2}C_2$ solid solution. *J Am Ceram Soc*. 2012;95:102.
40. Vegard L. Die Konstitution der Mischkristalle und die Raumfüllung der Atome. *Z Phys*. 1921;5:17.
41. Murphy ST, Chroneos A, Jiang C, et al. Deviations from Vegard's law in ternary III-V alloys. *Phys Rev B*. 2010;82:073201.
42. Lapauw T, Tytko D, Vanmeensel K, et al. $(Nb_{-x}, Zr_{1-x})(4)AlC_3$ max phase solid solutions: processing, mechanical properties, and density functional theory calculations. *Inorg Chem*. 2016;55:5445.
43. Sanchez-Portal D, Artacho E, Soler JM. Projection of plane-wave calculations into atomic orbitals. *Solid State Commun*. 1995;95:685.
44. Mulliken RS. Electronic population analysis on LCAOMO molecular wave functions. I. *J Chem Phys*. 1955;23:1833.
45. Gou H, Hou L, Zhang J, et al. Pressure-induced incompressibility of ReC and effect of metallic bonding on its hardness. *Appl Phys Lett*. 2008;92:241901.
46. Hadi MA, Ali MS, Naqib SH, et al. Band structure, hardness, thermodynamic and optical properties of superconducting Nb_2AsC, Nb_2InC and Mo_2GaC. *Int J Comp Mater Sci Eng*. 2013;2:1350007.
47. Gao FM. Theoretical model of intrinsic hardness. *Phys Rev B*. 2006;73:132104.
48. Westbrook JH, Conrad H. *The Science of Hardness Testing and Its Research Applications*. Ohio, USA: ASM; 1973.
49. Szymański A, Szymański JM. *Hardness Estimation of Minerals Rocks and Ceramic Materials*. Amsterdam, Holland: Elsevier; 1989.
50. Glazov VM, Vigdorovid VN. *Hardness of Metals*. Moskva, URSS: Izd. Metellurgiya;1989.
51. Dubois S, Bei GP, Tromas C, et al. Synthesis, microstructure, and mechanical properties of $Ti_3Sn_{(1-x)}AlxC_2$ MAX phase solid solutions. *Int J Appl Ceram Tech*. 2010;7:719.
52. Tzenov NV, Barsoum MW. Synthesis and characterization of Ti_3AlC_2. *J Am Ceram Soc*. 2000;83:825.
53. Tromas C, Chen JX, Wang JY. Strengthening of Ti_3AlC_2 by incorporation of Si to form $Ti_3Al_{1-x}Si_xC_2$ solid solutions. *Acta Mater*. 2006;54:1317.

54. Han JH, Hwang SS, Lee D, et al. Synthesis and mechanical properties of Ti_3AlC_2 by hot pressing TiC_x/Al powder mixture. *J Eur Ceram Soc*. 2008;28:979.
55. Ali MS, Islam AKMA, Hossain MM, et al. Phase stability, elastic, electronic, thermal and optical properties of $Ti_3Al_{1-x}Si_xC_2$ ($0 \leq x \leq 1$): first principle study. *Phys B*. 2012;407:4221.

How to cite this article: Zapata-Solvas E, Hadi MA, Horlait D, et al. Synthesis and physical properties of $(Zr_{1-x},Ti_x)_3AlC_2$ MAX phases. *J Am Ceram Soc*. 2017;100:3393–3401. https://doi.org/10.1111/jace.14870